ELSEVIER

Journal of Archaeological Science 32 (2005) 841–853

Journal of Archaeological SCIENCE

http://www.elsevier.com/locate/jas

Quantitative analysis of shape attributes based on contours and section profiles in artifact analysis

Idit Saragusti[a], Avshalom Karasik[a,b,*], Ilan Sharon[b], Uzy Smilansky[a]

[a] *Department of Physics of Complex Systems, The Weizmann Institute of Science, Rehovot 76100, Israel*
[b] *Institute of Archaeology, The Hebrew University, Jerusalem 91904, Israel*

Received 19 February 2004; received in revised form 5 December 2004

Abstract

Shape attributes, which are significant in various branches of archaeological research, are usually deduced from the study of planar contours or cross sections. We present here a new approach to contour analysis, which enables us to quantify in a well-defined way significant shape properties that are often used to describe artifacts – symmetry, deformation, roughness, etc. It is meant to replace traditional, often impressionistic shape descriptions.

Keywords: Shape analysis; Mathematics in archaeology; Handaxes

1. Introduction

The description and analyses of the *shapes* of artifacts are basic to most archaeological studies. Commonly, classifications of stone artifacts and ceramic vessels, for example, rely mostly if not entirely on various attributes of the shapes of these artifacts. In many cases, one can obtain sufficient information about the objects by considering their sections, profiles or projections on selected planes. In this way, the description of the three dimensional object is reduced to that of a planar curve. Profiles of prehistoric stone artifacts and sections of pottery are indeed the most common, but by no means the only examples. In a previous paper published by our group, we demonstrated how the application of mathematical methods for the analysis of curves could be useful in typological classifications of ceramics [10]. Such classifications may rely on the form of the entire shape of the vessels, or on selected parts considered to be significant for typological classification, such as rims, handles, etc. In the current paper, we wish to extend this idea, and to use similar methods for quantitative analyses of specific shape attributes, which are often used to describe characteristic features of archaeological interest, and which cannot be derived from few measurements. Our aim is to replace the vocabulary of *descriptive* terms, with quantities which are *unambiguously* defined; to quantify the intuitively appealing, yet imprecise, terminology often found in archaeological publications.

As in Ref. [10] the approach here is based upon the analysis of the curve as a whole. However, the method presented there – the use of the *curvature function* – is here extended to a *family* of similar functions, each analyzing the curve in a different way. In all these functions, the entire information about the curve is stored, but each function emphasizes different features by giving them more weight than others. The choice of

* Corresponding author. Department of Physics of Complex Systems, The Weizmann Institute, Rehovot 76100, Israel. Tel.: +972 8 93 44 987; fax: +972 8 93 44 109.
E-mail address: fekarasi@wisemail.weizmann.ac.il (A. Karasik).

0305-4403/$ - see front matter © 2005 Elsevier Ltd. All rights reserved.
doi:10.1016/j.jas.2005.01.002

one function over another is dictated by the specific application/problem at hand. This is where archaeological considerations and constraints come into play.

The shape attributes particularly addressed in this paper are symmetry, roughness and deformation. These are significant in many archaeological cases and are thus employed here to demonstrate how the mathematical methods can be applied for quantitative analysis. Yet, we wish to emphasize that our approach is general in the sense that it can be applied for quantifying many other shape attributes of interest.

In the next sections we explain our approach and illustrate it in several applications. We start the discussion with a brief overview of some mathematical concepts that are used to quantify line shape attributes. We tried to provide a self-contained exposition, which is aimed for readers with minimal mathematical background. The next step is to use these concepts to quantify specific shape properties of the lines. Each of these properties is discussed separately, and its archaeological relevance explicated by applying the analysis to one or more specific archaeological case studies. Our main goal here is to present the methods and their potential applicability in archaeological research. We therefore present only brief overviews of the archaeological context of each of these case studies, and do not discuss the interpretations of the results.

2. Planar curves

A general way to define a curve in the plane is by providing the coordinates of each point on the curve $(x(s), y(s))$, where s denotes the arc-length along the curve. As the parameter s changes, the point moves along the line. In the applications that concern us here, each artifact is represented by a single (connected) curve of length L, which does not intersect itself. For such curves, the coordinate functions are L-periodic functions of s. (We follow the standard convention, that while advancing on the curve in the direction of increasing s, the interior is always to the left.) This approach of looking at arc-length functions avoids the problems of non-uniqueness besetting previous attempts of parameterization of artifact-shapes by orthogonal or polar coordinates, e.g. [9,23]. At first glance it appears that this parameterization is uneconomical in as much as *two* functions are needed to describe a single series of points. However, the curve can be completely defined in terms of *either one* of these functions (to be referred to in the sequel as the *representation function*) from which the two coordinate functions $(x(s), y(s))$ can be computed by standard means. The reason why this is possible is illustrated in Fig. 1a.

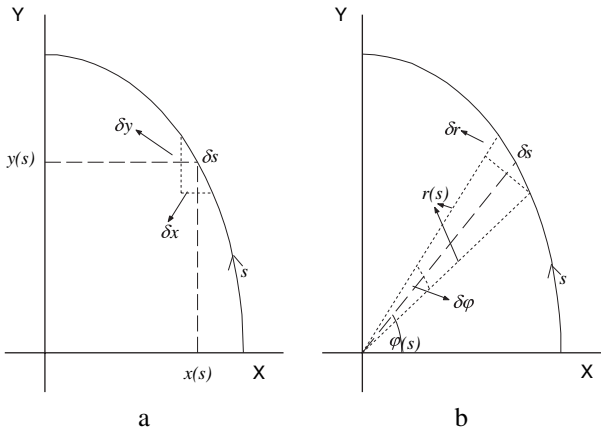

Fig. 1. Curve and two of its representations: the Cartesian (a) and the polar (b).

It shows that the small increments of the arc-length δs and of the coordinates increments along the curve, δx and δy, are related by

$$(\delta s)^2 = (\delta x)^2 + (\delta y)^2. \tag{1}$$

This relation, alongside the representation function provides the two relations from which the two coordinates can be computed. We shall use the following representations, whose definitions are illustrated in Figs. 1 and 2.

2.1. The Cartesian representation

As was explained above, the knowledge of $x(s)$ suffices to recover the curve. Writing $\delta x = (\mathrm{d}x/\mathrm{d}s)\delta s$, Eq. (1) can be used to obtain $\delta y = \sqrt{1-(\mathrm{d}x/\mathrm{d}s)^2}\delta s$. This determines the curve, since now both increments δx and δy are rendered in terms of δs. The Cartesian representation is naturally called for in the description of pottery profiles, where $x(s)$ can be chosen as the distance from the axis of cylindrical symmetry of the vessel. A profile of a simple vessel and its Cartesian representation are shown in Fig. 2a and b.

2.2. The polar representation

The polar coordinates, $(r(s), \varphi(s))$, give the distance r of a point on the curve from the origin, and φ is the orientation of the radius vector with respect to the x-axis (Fig. 1b). In this representation,

$$(\delta s)^2 = (\delta r)^2 + r^2(\delta\varphi)^2 \tag{2}$$

so that the knowledge of $r(s)$ determines the line. Indeed, writing $\delta r = (\mathrm{d}r/\mathrm{d}s)\delta s$ we obtain immediately $\delta\varphi = (1/r)\sqrt{1-(\mathrm{d}r/\mathrm{d}s)^2}\delta s$. This representation is

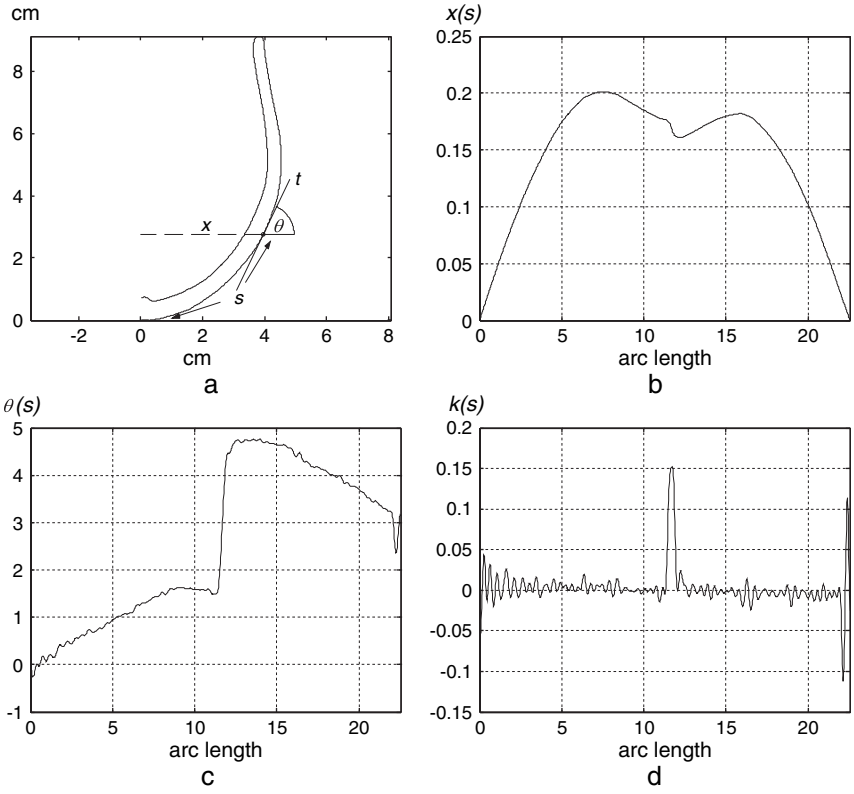

Fig. 2. A profile of a cup (a) and its representations: Cartesian (b), tangent (c) and curvature (d).

convenient for measuring deviations from circular shapes, since the representation of a circle is reduced to a very simple form, r = constant, $\varphi = 2\pi(s/L)$. If the curve to be discussed is convex, one could also describe the curve by the function $r(\varphi)$. This description cannot be used for general curves since a line in the φ direction may intersect the curve at more than one point so that $r(\varphi)$ is not uniquely defined. The latter representation was used previously by several authors [9,23]. They chose the center of gravity as the origin, and measured $r(\varphi)$ at a discrete set of angles.

2.3. The tangent representation

At each point on the curve we draw the tangent vector, which, by convention, points in the direction of increasing s (see Fig. 2a). We denote by $\theta(s)$ the direction of the tangent vector with respect to a fixed axis (for simplicity the axis can be chosen as the x-axis). The tangent angle $\theta(s)$ determines the curve since $\delta x = \cos\theta(s)\delta s$ and $\delta y = \sin\theta(s)\delta s$. The last relation enables us to express the tangent angle in terms of the Cartesian coordinates $\theta(s) = \arctan((\mathrm{d}y/\mathrm{d}s)/(\mathrm{d}x/\mathrm{d}s))$. Note that for closed curves, $\theta(s)$ increases by 2π upon a complete traversal of the curve. However, the function $\Delta\theta(s) = \theta(s) - 2\pi(s/L)$ is periodic and it will be used on some occasions. An illustration is given in Fig. 2c. The tangent representation was already used in Refs. [20,24], but the advantages offered by considering the arc-length to determine the position on the curve were not noticed.

2.4. The curvature representation

The curvature $\kappa(s)$ measures the rate of change of the tangent angle: $\kappa(s) = (\mathrm{d}\theta/\mathrm{d}s)$. An alternative definition can be given in terms of the radius $\rho(s)$ of the circle that osculates the curve at the point s: $\kappa(s) = 1/\rho(s)$. The advantage of this representation is that $\kappa(s)$ is large where the line changes its direction in the most rapid way, which are also the points of greatest interest in many archaeological applications (see Fig. 2d). This representation was discussed and used in several papers [10,15,22,27].

Before closing this section, we would like to emphasize an important property that is common to all the representations listed above: each of them provides the *complete information* about the curve (excluding trivial shifts or rotation of the coordinate axes). In other words, the curve and each of its representations are in a one-to-one relation.

If the representations are all equivalent how does one choose between them? The answer is to be found in the nature of the specific features of the line that are of interest in specific cases. The Cartesian and the polar

representations provide the large-scale features of the curve. A small indentation that only changes the curve locally will appear as a small perturbation in these representations. The tangent angle depends more strongly on local features (it is defined as a ratio of derivatives of the Cartesian coordinates), and hence, local changes of the line will show up. The curvature involves a higher derivative, and thus it is very sensitive to local variations. The features of the line that provide information on the gross properties of the curve will be hardly shown. This is illustrated in Fig. 2, where the small indentation at the bottom of the cup interior (the vicinity of the largest s values) is hardly visible in the Cartesian representation, but becomes a dominant feature in the tangent and even more so in the curvature representations. Thus, the selection of the representation to be used is dictated by the particular application at hand, and on the features of the curve which are of relevance. The considerations that determine this choice are illustrated below by few examples.

So far we treated the curves as if they are provided in the form of continuous functions. In most applications, however, the curves are rendered as discrete sets of points (pixels, poly-lines of x,y measurements, etc.). In Appendix we describe a convenient way to transcribe the discrete data into a form where the formalism presented above can be used.

3. Shape attributes of archaeological interest

In the present section, we address three different shape attributes and define them in terms of one of the representations listed above. To avoid abstract discussion, we develop the concepts in close relation to real archaeological applications.

3.1. Mirror (reflection) symmetry

A curve in the plane is symmetric under reflection if there is a line (symmetry axis) that divides the curve into two parts, which are mirror images of each other with respect to the symmetry axis. If the objects one investigates are not exactly symmetric, we would like to find the best reflection axis for which one achieves the *minimal* difference between one side and the reflection image of the other side. The degree of [a]symmetry of artifacts is often an attribute of interest in archaeology. The value of the minimal difference from perfect symmetry for a given object is taken as a measure of the *asymmetry*. We illustrate the application of this measure in two different contexts. The first is an assemblage of Lower Paleolithic handaxes, which are represented here by the outlines (projection) of their plan-view boundaries. Line-drawings of handaxes plan-view contours and their best symmetry axes are shown in Fig. 3. The second example is a group of modern ceramic flower-pots for which several profiles were measured (see Fig. 5) and the symmetry axis was used to identify the best rotation axis of each pot.

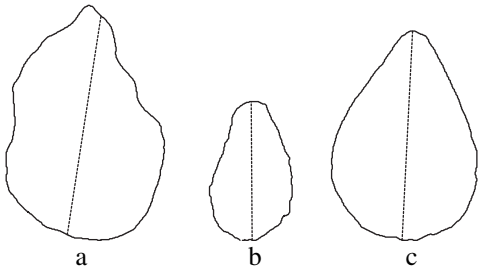

Fig. 3. Handaxes plan-view contours from 'Ubeidiya (a), Gesher Benot Ya'aqov (b) and Ma'ayan Barukh (c) with their best symmetry axis (dashed line). The asymmetry values are 0.00119, 0.00088 and 0.00029, respectively.

To define the asymmetry, it is helpful to consider first a symmetric curve. The axis of symmetry intersects the curve at two points s_0 and $s_0+(L/2)$. Points at a distance Δs in front or behind s_0 are mirror symmetric, and therefore have equal curvatures:

$$\kappa(s_0-\Delta s)=\kappa(s_0+\Delta s). \tag{3}$$

Equivalently, the change in the tangent angle between the point $s_0-\Delta s$ to the reflection point s_0 is the same as the change in the tangent angle from s_0 to the symmetric point $s_0+\Delta s$:

$$\theta(s_0)-\theta(s_0-\Delta s)=\theta(s_0+\Delta s)-\theta(s_0). \tag{4}$$

Similar identities can be written for the Cartesian and the polar representations. We shall discuss only the tangent and the curvature representations because they were used in the examples below.

For curves that are not perfectly symmetric, both Eqs. (3) and (4) above will be violated. To proceed, one must first choose the representation in which the asymmetry is to be determined. If the archaeological considerations assign more emphasis to the symmetric arrangement of corners, indentations etc. the curvature is preferred. If the general appearance of the line is more important, one had better use the tangent representation. *The best axis of symmetry and the value of the asymmetry naturally depend on the representation*. In the sequel, we provide the asymmetry in both representations, though in the examples discussed here the tangent angle was found more appropriate.

The symmetry axis is defined by the point s_0 (and its conjugate $s_0+(L/2)$), for which either Eqs. (3) or (4) are minimally violated. To this end we define the function $A_\kappa(\tilde{s})$, which measures to what extent Eq. (3) is not

satisfied when a point $\tilde{s}$ is assumed to be the symmetry point,

$$A_\kappa(\tilde{s}) = \int_0^{L/2} \left(\kappa(\tilde{s}+s) - \kappa(\tilde{s}-s)\right)^2 \mathrm{d}s. \quad (5)$$

Similarly, we define the extent by which Eq. (4) is violated with respect to the point $\tilde{s}$ by using the function

$$A_\theta(\tilde{s}) = \int_0^{L/2} \left(\theta(\tilde{s}+s) + \theta(\tilde{s}-s) - 2\theta(\tilde{s})\right)^2 \mathrm{d}s. \quad (6)$$

The optimal reflection axis is determined by the point s_κ at which $A_\kappa(s_\kappa)$ is minimal, or a point s_θ where $A_\theta(s_\theta)$ is minimal. The residual difference provides the deviation of the shape from perfect symmetry – which is the quantity we are after. We shall now turn to the examples.

3.1.1. Example 1: the degree of symmetry of contours of handaxes

Our first example for an archaeological issue in which symmetry is a significant shape property is the description and classification of handaxes. Handaxes first appeared around 1.6–1.7 million years ago, were gradually distributed over wide geographical extents, and remained an important part of the hominids' toolkit till the end of the Lower Paleolithic. Since they were produced for a very long period of time and can be found throughout most of the Old World, their description and classification are instrumental in addressing a large variety of issues. To a large extent such studies are based on general morphological typology, and analyses of specific shape attributes. Among the latter, the degree of symmetry and the degree of regularity of the contours of handaxes are considered to be of particular relevance. It is commonly accepted that the degree of symmetry generally increased over time, while the degree of irregularity or roughness decreased (see below). These chronological trends, in turn, are often interpreted as resulting from, and thus as manifestations of significant developments in human cognitive, behavioral and technological capacities (e.g. [16,35] and see also an overview in Ref. [32]). Yet, despite their significance, available methods for the characterization of handaxes are still based on traditional typologies (e.g. [6]) and/or metric measurements (e.g. [29,30]). They fail to deal with these shape properties in a quantitative way [32]. The general methods proposed here are able to satisfy these needs.

To test the hypothesis that handaxes became more symmetric over time, we applied the method described above for the analysis of the degree of symmetry of handaxes from five contexts, which represent various chronological stages in the Lower Paleolithic of the Levant. These are, from earliest to the latest: 'Ubeidiya (UB; n = number of objects =45) is a Lower Pleistocene site that is currently dated to ca. 1.4 million years ago (mya) [5]. Gesher Benot Ya'aqov (GBY; $n = 96$) is dated to between 0.8 and 0.7 mya [13,34]. The Acheulian site of Ma'ayan Barukh (MB; $n = 50$) is not well dated, but it is fairly safe to argue that it is more recent than both UB and GBY (e.g., [11,12]). Finally, two samples from the Tabun cave, bed 90 and Layer E (denoted by T_{90} and T_e with $n = 45$ and $n = 79$, respectively). The T_e sample represents the final stage of the Lower Paleolithic and it is dated to ca. 0.35 mya, or later [14,26]. No absolute dates are yet available for bed 90 at the cave but it is stratigraphically lower, and thus definitely older than the T_e sample.

The best symmetry axes and asymmetry values were computed for all the samples using the tangent representation and minimizing the asymmetry function as given by Eq. (6). The resulting mean asymmetry values and their variances are shown in Fig. 4. To test our working hypothesis, the asymmetry values of the studied samples were compared, and tested statistically to identify any significant differences.

The results of the statistical analyses (using Tamhane's T2 pair-wise multiple comparisons test) exhibit statistically significant difference between the GBY and MB samples and all other samples. The three other samples, i.e. the UB and the two Tabun samples are not significantly different from each other.

As for the question of time-related trends in the asymmetry values: as can be clearly seen from the mean values of this variable (Fig. 4), the asymmetry values generally tend to decrease over time, i.e., *handaxes generally become more symmetric*. However, this trend is seen only among the UB, GBY and MB samples, representing most of the time range of the Lower Paleolithic, while the two Tabun samples, representing the end of the period, exhibiting higher values than could be expected considering their assumed ages, deviate from this general trend. The differences between the studied samples with respect to their asymmetry

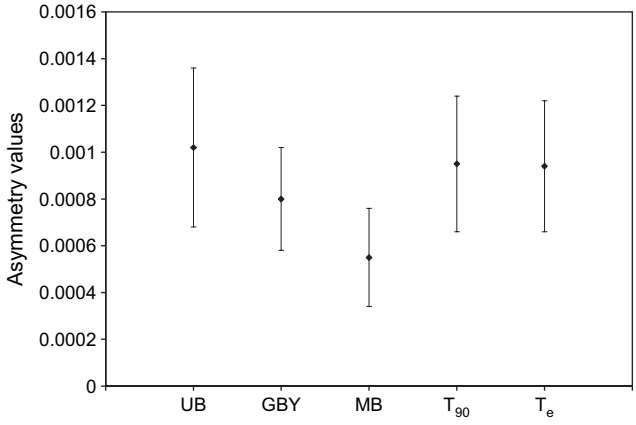

Fig. 4. Mean symmetry values of the five studied sites, and their standard deviations.

values are in some cases large and significant, while in others less so. In any case, the differences between the UB, GBY and MB samples, for which time-related trends are claimed, are statistically significant.

Another observation is that the *spread* of the plan-view asymmetry values generally decreases over time, as demonstrated by the standard deviation values (Fig. 4). Here again, the two samples from Tabun deviate from this general trend. In conclusion, the working hypothesis was generally confirmed by the analysis, yet the picture emerging is more complex than a simple monotonic increase in the degree of symmetry over time. It is beyond our scope here to interpret these results (for more details see [32]), but it is worth noting that the roughness of the same assemblage, to be discussed below, follows a similar trend. Moreover, the results presented here regarding the degree of symmetry are very similar to those previously published by two of us (and others coauthors) [33] and by one of us [32]. The results in those studies were obtained using different method for symmetry measurement, namely the Continuous Symmetry Measure (CSM) method [2,36], indicating that the measured degree of symmetry is an intrinsic property, unrelated to the means by which it is measured.

3.1.2. Example 2: the symmetry of two-sided profiles of modern ceramic flower-pots

One of the main assumptions underlying traditional analyses of ceramic profiles is that the vessels (especially when wheel-made) are cylindrically symmetric about the axis of revolution. Thus a single cross section suffices to characterize the entire vessel (but for added features like handles etc.). This assumption cannot be fully justified, and this is apparent when computerized methods are used to measure either the entire vessel, or several sections thereof [17,25]. To define the mean profile it is imperative to identify the axis about which the entire vessel is most symmetric. If, as in the example discussed here, a profilograph is used to digitize several *entire* (two-sided) cross sections of the same vessel (see Fig. 5), the determination of the rotation axis is reduced to the definition of the axis of mirror symmetry of each of the two-sided profiles, and later finding the mean over all the sections.

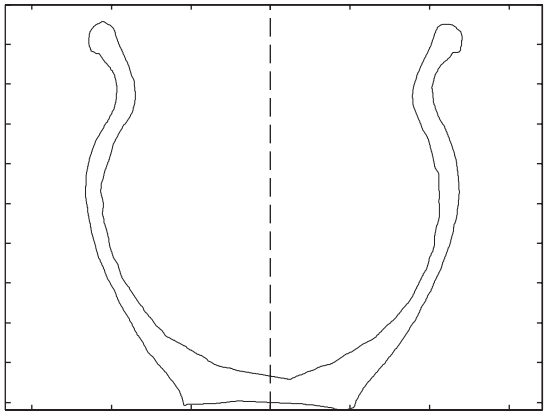

Fig. 5. A measured two-sided profile of a flower-pot, and the best mirror-symmetry axis.

The asymmetry was determined in the curvature representation (Eq. (5)), since here the rim and the base carination are of special significance. After determining the best symmetry axis, several other questions concerning the assemblage of flower-pots could be addressed, in particular, the degree of uniformity of each vessel and of the assemblage as a whole (see Ref. [17]). The mean asymmetry of each flower-pot was deduced and served as a quantitative measure of its deformation.

The fact that all the pots studied here showed a similar degree of asymmetry indicates a consistent flaw in the production technique - possibly a premature removal of the pots from the wheel.

There are many other examples in the archaeological research in which symmetry is a significant attribute. For instance, in a recent publication the authors attempted to reconstruct an excavated Gothic spire from its building blocks that were found scattered in the site. After recording the cross sections of the components, their relative alignment was determined by computing the symmetry axis of each section, and matching them in one direction [19].

3.2. Roughness (regularity)

The terms 'roughness' and 'regularity', which are often associated, are used in a rather ambiguous way in the archaeological literature. Sometimes, they indicate that the object is amorphous, and its shape deviates from well-defined 'classical' forms (i.e. 'ovate', 'tear-drop', etc.), while in other cases these terms are used to differentiate artifacts with rough contours from those having smoother ones. In this sense, 'regularity' is meant as a measure of the variations in corners, edges and faces [7, p. 411], or, simply a measure of directional changes [8, p. 205] in the object surface's (in three dimensions) or contour (in two dimensions). In the present study, we follow a similar definition of 'regularity' and refer to it in the sequel as 'roughness' (see below).

The method used here to quantify the degree of roughness of a given contour is based on the degree of *concavity* of this contour. The intuition at the root of this measure of roughness stems from the following observations: the smoothest closed curves are convex. Any further structure of the curve is associated with the appearance of concave sections: the more there are the more complex and rough the curve is. Thus, roughness can be determined by the frequency and amplitude of the transitions between *convex* and *concave* sections along the curve. These transitions occur at inflection *points* (Fig. 6). In terms of the *curvature function* introduced above, the *concavity* can be defined as the

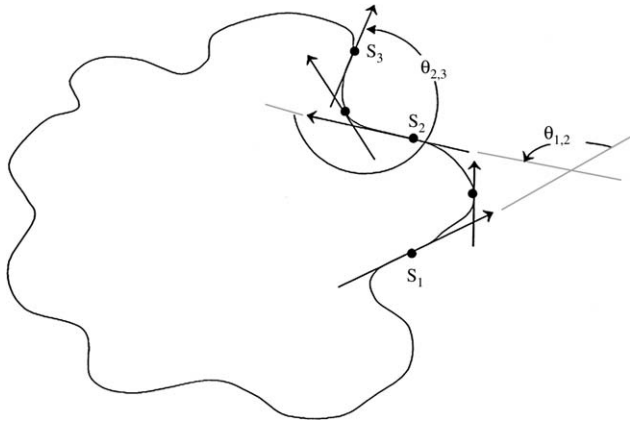

Fig. 6. Inflection points (S1,S2,S3), in a convex section (S1,S2) and in a concave section (S2,S3).

sum of all the deflections along concave sections. Formally,

$$C = \int_0^L |\kappa(s)| \frac{1 - \mathrm{sign}(\kappa(s))}{2} \, \mathrm{d}s \tag{7}$$

where $k(s)$ is the curvature at point s along the contour.

It should be borne in mind that *roughness is a relative term, and it depends upon the scale at which it is defined and measured*. This is analogous to the well-known question 'how long is the coast of Britain?' The answer depends on the yardstick by which it is measured, or in other words – depends upon the scale. A given line may look relatively smooth at one scale, and rougher as the resolution increases. Therefore, setting the scale at which the roughness is to be measured is a prerequisite in any quantitative assessment of its degree. The choice of scale is dictated by archaeological considerations, and may change when different properties are to be addressed. In comparative studies, however, the same scale should be used. It is convenient to set the scale by assessing the size of an arc along the curve, within which variations of the curvature are irrelevant and can be smoothed away. The largest scale of length in our problem is the circumference L. We define the length of the yardstick to be of length L/N_{eff}, where N_{eff} is an integer number. The fluctuations of the curve that occur on an interval of smaller length are damped out. This process is called smoothing and it is described in detail in Appendix. In the sequel, when we say "the degree of smoothing" we have in mind a specific choice of N_{eff}. The same curve can be observed at different smoothing levels. As N_{eff} is decreased, high-frequency oscillations are 'ironed' out, and the resulting curve appears smoother, and with a lower number of inflection points. We shall turn now to the examples.

3.2.1. Example 3: the roughness of the handaxes

The first example of an archaeological issue in which roughness is a significant shape attribute is taken again from the Lower Paleolithic handaxes. As already mentioned, the degree of regularity or roughness of handaxes is considered to have decreased over time [18], although, as far as we know, this was never tested in a quantitative way. The roughness analysis was performed on the same handaxe samples described above. To identify the desired scale at which handaxe roughness should be measured, we chose a few typical handaxes, on which significant variation in roughness could be determined visually, and their smoothed boundaries were compared at different levels. The smoothing level that was deemed to best represent the desired degree of roughness was the one that filtered out all oscillations considered too small, but left those of interest (Fig. 7).

Although there were few instances in which smoothing at this level 'ironed out' local features that might have been considered significant (see for example Fig. 7a_3), on average, this level seemed to be the most appropriate, and the scale at which the roughness was finally measured was $N_{\mathrm{eff}} = 10$.

Similarly to the symmetry analysis of handaxes, we tested the hypothesis that handaxes became less rough over time by comparing the five samples, with respect to

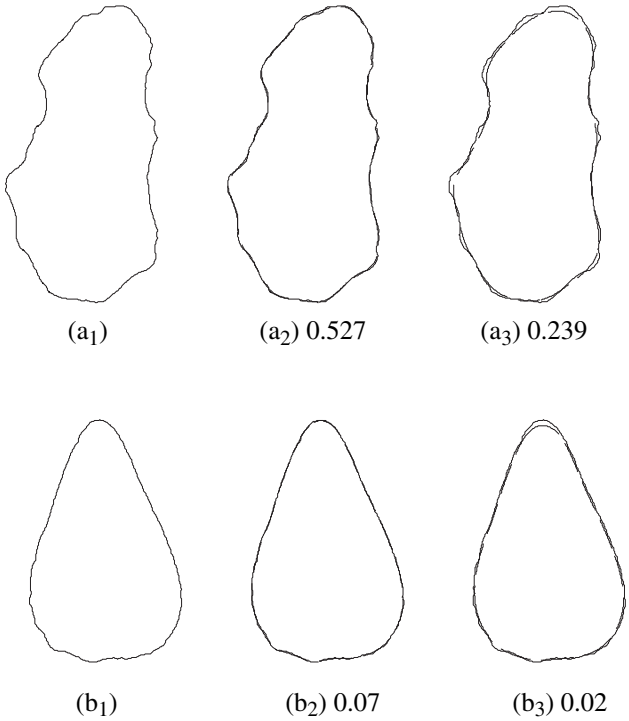

Fig. 7. Plan-view contours of handaxes from 'Ubeidiya (a_1) and Ma'ayan Barukh (b_1) the original contours (solid lines) and the smoothed contours at two different smoothing levels ($a_{2\&3}$, $b_{2\&3}$), (dashed lines). The roughness values at each level are given below.

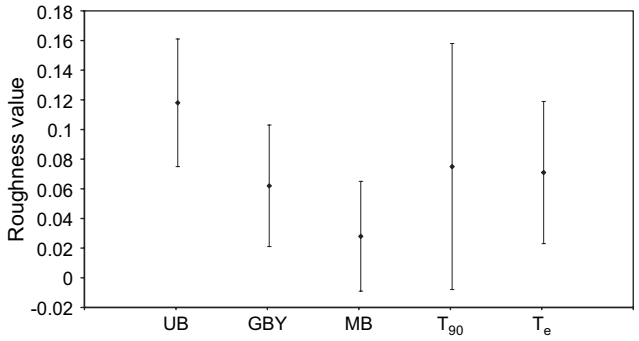

Fig. 8. The mean roughness of the five studied sites, and their standard deviation.

their degree of roughness. The mean roughness values and their variances are shown in Fig. 8.

Statistically significant differences were found between the UB and MB samples and all other samples (using the Tamhane's T2 pair-wise multiple comparison test). The three other samples, i.e. the GBY and the two Tabun samples are not significantly different from one another.

A time-related trend can be seen in the mean plan-view roughness values (Fig. 8). These values generally decrease over time, i.e. *the contours of the handaxes in their plan-view generally become less rough*. However, as in the case of the symmetry values, this trend is seen only among the UB, GBY and MB samples, while the two Tabun samples, exhibiting higher values than could be expected (considering their assumed ages), deviate from this general trend. The same time-related trend can be seen in the spread of the plan-view degree of roughness, as expressed by the standard deviation values (Fig. 8), with the two Tabun samples, once again, deviating from this trend. The consistency of the trends revealed in the analyses of the symmetry and the roughness of the samples probably is of archaeological significance and possible interpretations are discussed elsewhere [32].

3.2.2. Example 4: roughness analysis of phytoliths

Another issue in which we tried to test the applicability of our method of defining the concept of "roughness" is altogether different – the taxonomy of phytoliths. The analysis of phytoliths is becoming an increasingly important tool in archaeological research. The study of these microfossil plant remains can contribute significant information regarding the botanical remains at archaeological sites, especially at those sites in which phytoliths are the only plant remains found at excavations. These in turn are important for addressing questions regarding paleo-environment, paleo-economy etc. One of the main problems in phytoliths studies, however, is their taxonomic classification. This classification is based on the morphology of the phytoliths, and many attempts have been made to define shape attributes which can be used to distinguish between phytoliths of various taxa (e.g. [4]). T. Ball, for example, presented several morphological variables which can be used to distinguish between wheat and barley phytoliths [3]. We applied the methods described here, in cooperation with T. Ball, to look for morphological variables that can be used to distinguish between

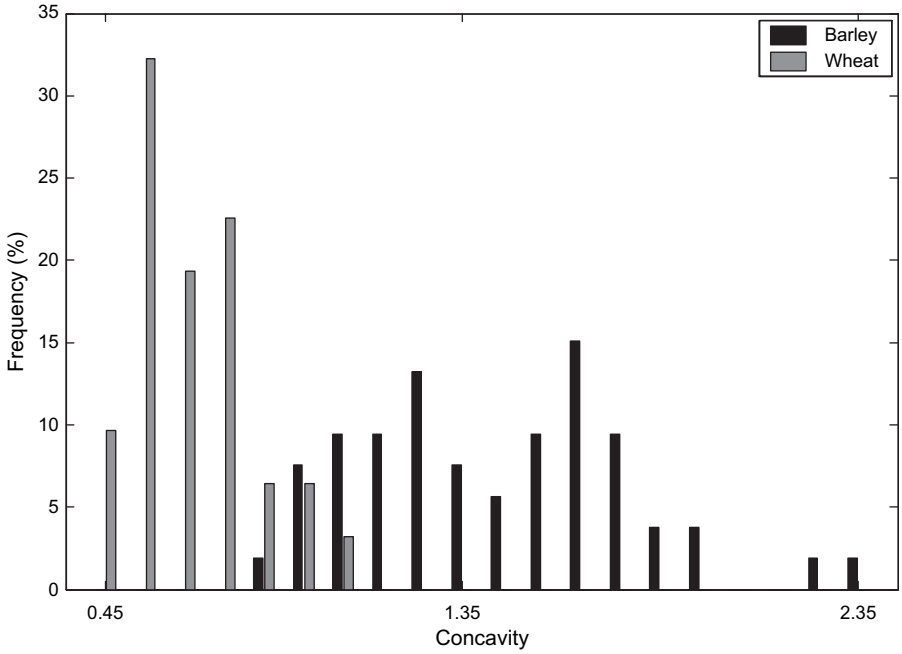

Fig. 9. Frequency distributions of concavity values of wheat and barley.

these two taxa. The preliminary results of this study are presented below.

The roughness of two sets of SEM images of wheat and barley phytoliths was measured in the same way as that of the handaxes, although the scale at which the phytoliths were measured was $N_{\text{eff}} = 40$.

The frequency distributions of the two types are given in Fig. 9. The Kruskal-Wallis test (used here because the distributions are non-normal) indicated that the difference between the two types is significant (<0.05). It can be therefore concluded that the degree of roughness (or 'concavity') can be used to clearly distinguish between the wheat and barley phytoliths.

Ball et al. [3] mentioned a similar variable – 'convexity' as one of the shape attributes that can be used to distinguish between the wheat and barley phytoliths. Our 'concavity' and their 'convexity' variables are similar but not identical. The convexity is the ratio between the convex perimeter of the curve and the entire perimeter. This definition, however, is not sensitive to the roughness introduced by the *magnitude* of the concave sections. Thus very shallow concave sections will have the same effect as very deep ones (if they are in the same length), and will contribute the same value to the overall convexity of the shape. The concavity, on the other hand, distinguishes between shallow and deep concave sections of the same lengths and their relative contribution to the final value will be different.

3.3. Deformations

Many artifacts, such as wheel-produced ceramics, are intended to be axially symmetric. Therefore, the boundaries of their intersections by planes that are perpendicular to the axis of rotation should be perfect circles (we shall use the term "horizontal sections" for these sections). However, these ideally symmetric objects may suffer deformations when still on the wheel, or during the drying and firing stages. As a result the aforementioned sections will deviate from perfect circles. The introduction of accurate measuring devices such as 3D scanning cameras [21,28,31] has made 3D representations of pottery available. Using these data, it is now possible to deduce the deformations of wheel-produced pottery. A systematic study of these deformations may reveal the technological flaws that induced them, and might possibly be used to characterize workshops methods and production patterns.

A quantitative measure of the deformations can be obtained by using the polar representation of the curves that are the boundaries of the horizontal sections. Fig. 10a shows the curves obtained by measuring two horizontal sections of a jug using a 3D camera. The jug in question is a closed and complete vessel and therefore the 3D camera provided only the horizontal section of its exterior surface. As can be seen in Fig. 10 (to be explained below), the curves are certainly not the ideally expected concentric circles.

Our purpose here is to provide a quantitative measure of these deformations. The points on the curve are specified by their polar coordinates $(r(s), \varphi(s))$. For convex curves (and when the origin is in the interior) $\varphi(s)$ is a monotonic function of the arc-length s, and one can describe the curve by the function $r(\varphi)$ [9,23]. It is customary to use the Fourier coefficients of $r(\varphi)$

$$\hat{x}_n = \frac{1}{2\pi}\int_0^{2\pi} \mathrm{d}\varphi \cos n\varphi \; r(\varphi); \quad \hat{y}_n = \frac{1}{2\pi}\int_0^{2\pi} \mathrm{d}\varphi \sin n\varphi \; r(\varphi)$$

to define the nth deformation parameter and associated phase by

$$r_n = \sqrt{\hat{x}_n^2 + \hat{y}_n^2}; \quad \alpha_n = \arcsin\left(\frac{\hat{x}_n}{r_n}\right).$$

The deformation parameters are determined in an unambiguous way when we choose the origin such that the coefficients $\hat{x}_1$ and $\hat{y}_1$ vanish. For simple shapes, this choice is equivalent to setting the origin at the center of gravity of the curve. The parameter r_0 is the mean radius, and it serves to set the scale (size) of the section. The first non-trivial coefficients $(\hat{x}_2, \hat{y}_2)$ or equivalently (r_2, α_2) determine the parameters of the ellipse which fits the curve best: r_2/r_0 is proportional to the eccentricity and α_2 is the tilt angle of the main axes of the ellipsoid relative to the coordinate axes. The higher order parameters provide information on deformations on smaller scales. When the curve is not convex, $\varphi(s)$ is not necessarily monotonic, and therefore one has to define the Fourier transform in another way, which coincides

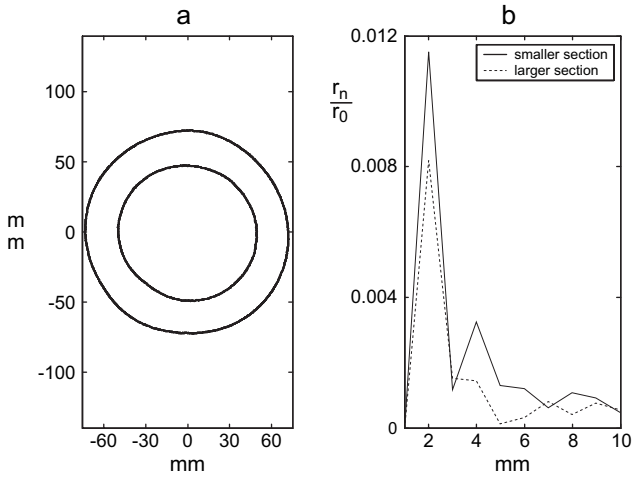

Fig. 10. (a) Two horizontal sections of the jug shown on the left in Fig. 11. (b) The leading 10 Fourier coefficients (scaled by r_0) of the sections shown in (a).

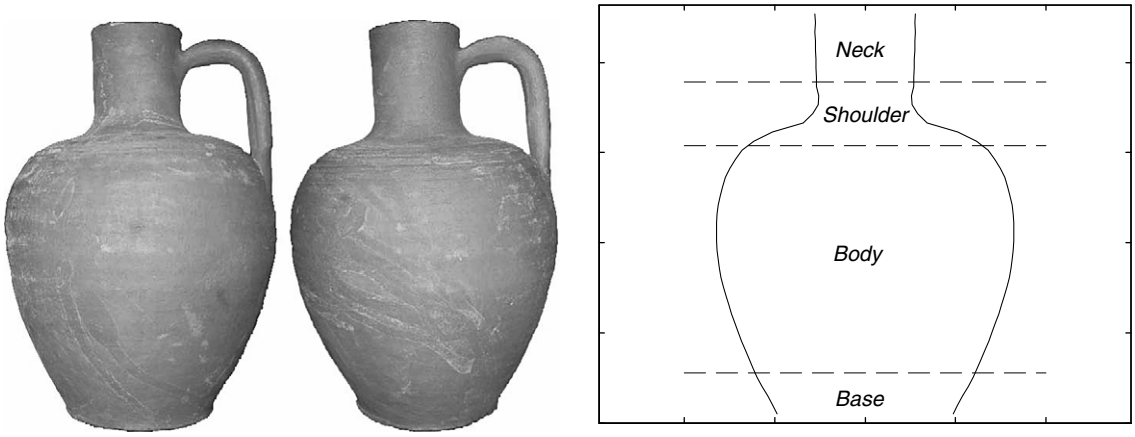

Fig. 11. Left: two similar wheel-made jugs from the market of Vienna. Right: a plan view of a jar where the four regions used in the current study is indicated.

with the definition above for convex curves. This can be simply done by changing the integration variable so that

$$\hat{x}_n = \frac{1}{2\pi}\int_0^L \mathrm{d}s \frac{\mathrm{d}\varphi}{\mathrm{d}s} \cos n\varphi(s)\; r(s);$$
$$\hat{y}_n = \frac{1}{2\pi}\int_0^L \mathrm{d}s \frac{\mathrm{d}\varphi}{\mathrm{d}s} \sin n\varphi(s)\; r(s).$$

Once this modification is introduced, the rest follows in the same way as in the discussion of the convex case. Fig. 10b shows the values of 10 scaled Fourier coefficients r_n/r_0 for the sections shown in Fig. 10a.

To demonstrate the potential value of the study of deformations in the archaeological context we discuss below a case study in which the deformation of the horizontal sections can yield information relevant to the manufacturing process of the ceramic vessels.

3.3.1. Example 5: deformations of contemporary wheel-made jugs

Two contemporary but traditionally-produced wheel-made jugs were scanned by a 3D scanner, which provides a complete three dimensional digital representation of the studied object, from which the horizontal sections at various heights were computed [1,31]. This detailed information was used to determine various quantities that are relevant to the shape of the objects and their deviations from cylindrical symmetry [25].

Here we shall only discuss the information provided by the 10 leading Fourier coefficients computed for 45 different horizontal sections for each of the jugs. Even though the two jugs look rather similar, their averaged scaled Fourier coefficients r_n/r_0 are quite different, as can be seen in Fig. 12; the right hand jug is more deformed than the one on the left.

The detailed investigation to be discussed below reveals that the deformation is not uniform along the jar, which indicates that different parts underwent different types of stress and pressure before the final shape was set. To reach this conclusion we analyzed the deformations by dividing the 45 horizontal sections into 4 groups (Fig. 11 right): (1) *the neck* (upper 8 horizontal sections); (2) *the shoulder* (the next 7 sections); (3) *the body* (the next 25 sections); and (4) *the base* (the lowest 5 sections). Some horizontal sections include the handle. Therefore, in all sections we used the points on the 180° arc opposite the handle. The mean scaled Fourier coefficients for each group were computed, and they are shown in Fig. 13. The body of the two jars is the closest to perfect circles. This implies that the deviations from perfect symmetries were not caused by external pressure such as induced by e.g., too crowded packing of the kiln. The deformation pattern of the two jars is different. The right hand jug is *more* deformed as far as the neck and shoulders are concerned, although its base is *less* deformed than the base of the other jug. On the other hand, the base of the left hand jug is more deformed than

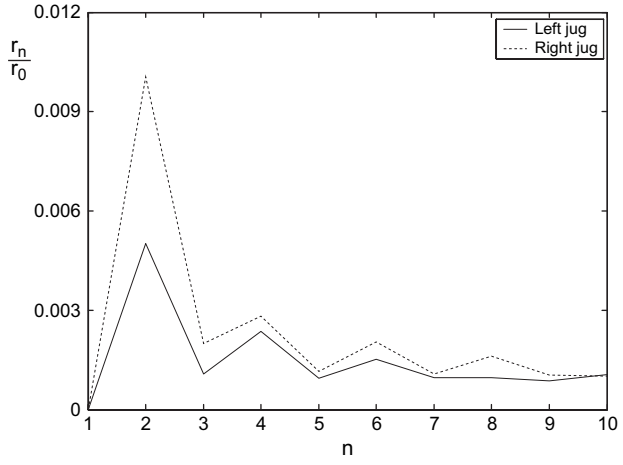

Fig. 12. The mean scaled Fourier coefficients for the two jugs averaged over the entire height.

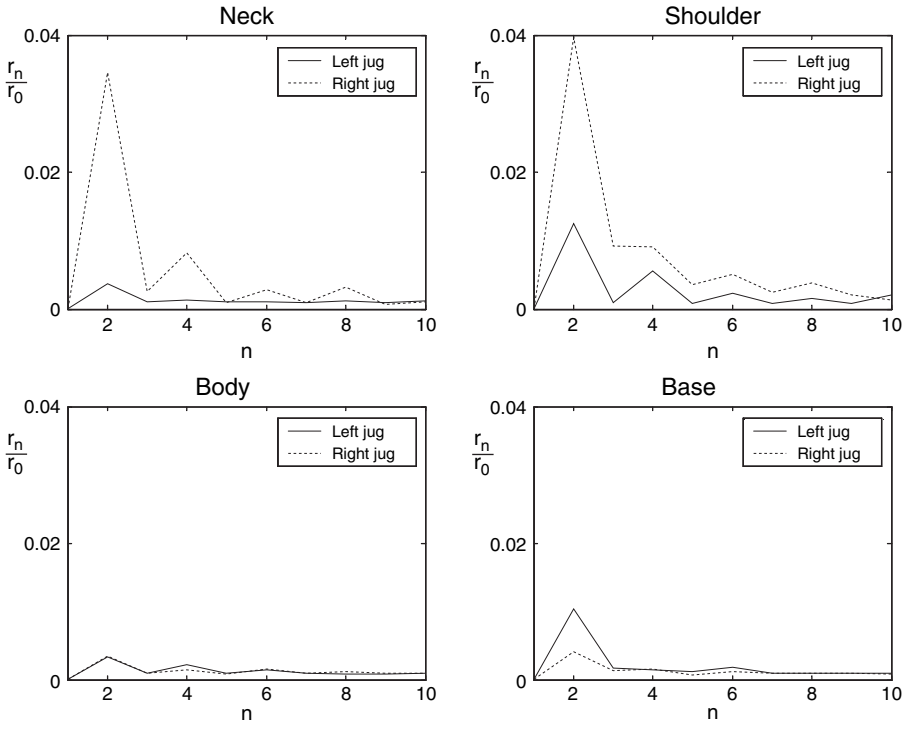

Fig. 13. The normalized Fourier coefficients for the separated parts of the two jugs.

the one on the right jug (although on a smaller scale). Previous analysis showed that the most significant deformation of the neck is probably due to the attachment of the handle, which was pressed onto the still soft neck and deformed it. The difference between the two neck deformations can be explained by the application of stronger force when the potter attached the handle to the right hand jug. Such action would break the circular symmetry of the vessel, but would preserve the mirror symmetry about the line which crosses through the handle (see Ref. [25] for further details).

Even if the potter produced similar vessels, as can be suggested by the low deformation values of the body, he deformed them in different ways while he added decoration, handles or removed them to be dried elsewhere. The deformations of the shoulder regions are probably due to the material tensions which is expected in places where the surface is of highest curvature.

The differences between the jugs were noticed only through the Fourier deformation analysis and could hardly be traced by eye. Their measurements, which are possible with the use of high-resolution 3D devices, may provide the archaeologists with valuable information regarding the technology of ceramics.

4. Concluding remarks

Our main purpose in the current paper was to introduce to the archaeological audience several mathematical methods for the description of closed curves, and to demonstrate how these methods can be applied for the analyses of various shape attributes that are considered to be significant for archaeological research. The mathematical methods, briefly outlined in part II, allow the reduction of the entire information about the curves to single functions. Each of these functions is sensitive to different properties of the curve, thus emphasizing different features. Choosing the most appropriate function to the nature of the curves under study and to the specific archaeological problem at hand, one can then use these functions for *quantitative* analyses of various shape attributes of interest. Examples from the archaeological realia for such attributes were provided in part III. It was demonstrated how specific shape attributes, such as symmetry, roughness and deformation, can be measured using these functions. The advantage of quantitative analyses of such attributes is self-evident. Moreover, the approach presented in this paper is general and sufficiently versatile in the sense that it can be used to describe *any* curve of interest (under the limitations mentioned above), and many other shape attributes can be quantitatively analyzed using methods such as those described here.

Acknowledgements

This research was supported by a BIKURA grant from the Israel Science Foundation, by the Kimmel Center

for Archaeological Sciences and the J&R Foundation in the Weizmann Institute of Science. We wish to thank N. Goren-Inbar, O. Bar-Yosef, A Jelinek and A. Asaf for permitting us to analyze the handaxes from the studied sites, to H. Mara for the 3D data and to A. Gilboa and D. Zukerman for their helpful comments. I.S. also wishes to thank D. Avnir, M. Pinski and O. Katzenelson for their enormous help.

Appendix

In practical applications, the information about the curve to be analyzed is provided in a form of a list of coordinates (x_i, y_i), $i = 1, \ldots, N$ of points on the curve. If the input for analysis is a raster image (e.g., a scan) these would be the outer pixels of the object in the image, and in a vector representation (e.g., a profilograph connected to an AutoCAD system) they would be the direct (x,y) coordinates measured by the system. The discrete representation must be converted into a smooth function so that the formulae presented in the preceding sections can be used. Since in many applications the curves are closed, the Fourier interpolation is a natural candidate for the required transformation, although it can also be used with small modifications for curves that are not closed.

Assuming that the coordinates are provided in an ordered way (that is, the point denoted by the index i lies on the curve between the points $i-1$ and $i+1$), we can compute the arc-length difference between successive points by

$$\delta s_{i+1} = \sqrt{(x_{i+1} - x_i)^2 + (y_{i+1} - y_i)^2}.$$

The arc-length to the point i is computed by $s_i = \sum_{j=1}^{i} \delta s_j$, where the reference point from which the arc-length is measured is the point with index $i = 1$. If the arc-length intervals δs_i vary from point to point, it is convenient to shift the points along the curve so that the arc-length differences are constant and equal L/N where L is the length of the entire line. This is achieved by interpolating the coordinate vectors. At the end of this process we obtain the new coordinate vectors (x_i, y_i) of equidistant points on the curve. Denoting the discrete Fourier transform of the vectors x_i and y_i by $(\hat{x}_n^{(x)}, \hat{y}_n^{(x)})$ and $(\hat{x}_n^{(y)}, \hat{y}_n^{(y)})$ (respectively), $n = 1, \ldots, N$, we obtain the curve in the form

$$\begin{aligned} x(s) &= \hat{x}_0^{(x)} + \sum_{n=1}^{N} \left(\hat{x}_n^{(x)} \sin\frac{2\pi n}{L}s + \hat{y}_n^{(x)} \cos\frac{2\pi n}{L}s \right) \\ y(s) &= \hat{x}_0^{(y)} + \sum_{n=1}^{N} \left(\hat{x}_n^{(y)} \sin\frac{2\pi n}{L}s + \hat{y}_n^{(y)} \cos\frac{2\pi n}{L}s \right). \end{aligned} \tag{A.1}$$

The wavelength of the nth term in the above expansion is L/n, and hence, as n increases, finer details of the function are resolved. The finest details usually reflect the numerical noise introduced by the errors in the measurement of the original coordinates, the roughness introduced by the use of rectangular pixels in raster representation of the image, the truncation of least-significant digits by the computer, etc. Thus, further smoothing is called for. Smoothing is also required in certain applications when the quantity of interest depends in an intrinsic way on the scale at which it is observed. This point was discussed when we introduced the definition of "roughness" in terms of the concavity. We introduced the smooth version of the data by replacing the Eq. (A.1) by

$$\begin{aligned} x(s) &= \hat{x}_0^{(x)} + \sum_{n=1}^{N} w_n \left(\hat{x}_n^{(x)} \sin\frac{2\pi n}{L}s + \hat{y}_n^{(x)} \cos\frac{2\pi n}{L}s \right) \\ y(s) &= \hat{x}_0^{(y)} + \sum_{n=1}^{N} w_n \left(\hat{x}_n^{(y)} \sin\frac{2\pi n}{L}s + \hat{y}_n^{(y)} \cos\frac{2\pi n}{L}s \right). \end{aligned} \tag{A.2}$$

where the weights $w_n = 1/(1+\exp[1+(n - N_{\mathrm{eff}})/\Delta])$ are chosen such that $w_n \approx 1$ for $n < N_{\mathrm{eff}}$, and $w_n \to 0$ as n increases beyond N_{eff}. The transition occurs in a gradual way on an n interval of size Δ. Thus, the value of N_{eff} determines the smoothing level: details on the scale smaller than L/N_{eff} are neglected at this smoothing level. (In the analysis reported here we chose $N_{\mathrm{eff}} = 10$, 40 and $\Delta = 2$.)

References

[1] K. Adler, M. Kampel, R. Kastler, M. Penz, R. Sablatnig, K. Schindler, S. Tosovic, Computer aided classification of ceramics – achievements and problems, in: Proceedings of Sixth International Workshop on Archaeology and Computers, Vienna, Austria, 2001.

[2] D. Avnir, O. Katzenelson, S. Keinan, M. Pinsky, Y. Pinto, Y. Salomon, H. Zabrodsky Hel-Or, The measurement of symmetry and chirality, in: D.H. Rouvray (Ed.), Concepts in Chemistry, Research Studies Press, Somerset, 1996, pp. 283–324.

[3] T. Ball, J.S. Gardner, N. Anderson, Identifying inflorescence phytoliths from selected species of wheat (*Triticum monococcum*, *T. dicoccon*, *T. dicoccoides*, and *T. aestivum*) and Barley (*Hordeum vulgare* and *H. spontaneum*) (Gramineae), American Journal of Botany 86 (1999) 1615–1623.

[4] T. Ball, J.S. Gardner, J.D. Brotherson, Identifying phytoliths produced by the inflorescence bracts of three species of wheat (*Triticum monococcum* L., *T. dicoccon* Schrank., and *T. aestivum* L.) using computer-assisted image and statistical analyses, Journal of Archaeological Science 23 (1996) 619–632.

[5] O. Bar-Yosef, N. Goren-Inbarin: The lithic assemblages of 'Ubeidiya, a Lower palaeolithic site in the Jordan valley, vol. 34, The Institute of Archaeology, the Hebrew University of Jerusalem, Jerusalem, 1993.

[6] F. Bordes, Typologie du Paleolithique Ancien et Moyen, Presses du CNRS, Paris, 1961.

[7] M. Diepenbroek, A. Bartholoma, H. Ibbeken, How round is round? A new approach to the topic 'roundness' by Fourier grain shape analysis, Sedimentology 39 (1992) 411–422.

[8] R. Erlich, B. Weinberg, An exact method for characterization of grain shape, Journal of Sedimentary Petrology 40 (1970) 205–212.

[9] J. Gero, J. Mazzullo, Analysis of artifact shape using Fourier series in closed form, Journal of Field Archaeology 11 (3) (1984) 315–322.
[10] A. Gilboa, A. Karasik, I. Sharon, U. Smilansky, Towards computerized typology and classification of ceramics, Journal of Archaeological Science 31 (2004) 681–694.
[11] D. Gilead, Early paleolithic culture in Israel and the Near East, Institute of Archaeology, The Hebrew University of Jerusalem, Jerusalem, 1970.
[12] D. Gilead, Handaxe industries in Israel and the Near East, World Archaeology 2 (1970) 1–11.
[13] N. Goren-Inbar, C. Feibel, K.L. Verosub, Y. Melamed, M. Kislev, E. Tchernov, I. Saragusti, Pleistocene milestones on the Out-of-Africa corridor at Gesher Benot Ya'aqov, Israel, Science 289 (2000) 944–947.
[14] R. Grun, C. Stringer, Tabun revised: revised ESR chronology and new ESR and U-series analyses of dental material from Tabun C1, Journal of Human Evolution 39 (2000) 601–612.
[15] M.B. Hagstrum, J.A. Hildebrand, The 'two-curvature' method for reconstructing ceramic morphology, American Antiquity 55 (2) (1990) 388–403.
[16] G.L. Isaac, Foundation stone: early artefacts as indicators of activities and abilities, in: G.N. Bailey, P. Callow (Eds.), Stone Age Prehistory, Cambridge University Press, Cambridge, 1986, pp. 221–241.
[17] A. Karasik, L. Bitton, A. Gilboa, I. Sharon, U. Smilansky, Quantitative measures of the uniformity of ceramics, in: Computers Applications and Quantitative Methods in Archaeology (CAA 2004), Prato, Italy, in press.
[18] M. Kohn, S. Mithen, Handaxes: products of sexual selection? Antiquity 73 (1999) 518–526.
[19] C. Laugerotte, N. Warzee, Computerised geometric analysis of a spire coming from a Gothic tabernacle, in: Computers Applications and Quantitative Methods in Archaeology (CAA 2004), Prato, Italy, in press.
[20] M.N. Leese, P.L. Main, An approach to the assessment of artefact dimension as descriptors of shape, in: J.G.B. Haigh (Ed.), Computer Applications in Archaeology 1983, University of Bradford, School of Archaeological Sciences, Bradford, 1983, pp. 171–180.
[21] F. Leymarie, D. Cooper, M.S. Joukowsky, B. Kimia, D. Laidlaw, D. Mumford, E. Vote, The SHAPE Lab. – new technology and software for archaeologists, in: Computing Archaeology for Understanding the past (CAA 2000), Archaeopress, Oxford UK, 2001, pp. 79–89.
[22] F. Leymarie, M.D. Levine, Curvature morphology, Computer Vision and Robotics Laboratory, McGill University, Canada, Montreal, Quebec, 1988.
[23] G. Liming, L. Hongjie, J. Wilcock, The analysis of ancient Chinese pottery and porcelain shapes: a study of classical profiles from the Yangshao culture to the Qing dynasty using computerized profile data reduction, cluster analysis and fuzzy boundary discrimination, in: Computer Applications and Quantitative Methods in Archaeology 1989, 1989, pp. 363–374.
[24] P. Main, Accessing outline shape information efficiently within a large database, in: S. Laflin (Ed.), Computer Applications in Archaeology 1986, Computer Center, University of Birmingham, Birmingham, 1986, pp. 73–82.
[25] H. Mara, R. Sablatnig, A. Karasik, U. Smilansky, The uniformity of wheel produced pottery deduced from 3D image processing and scanning, in: W. Burger, J. Scharinger (Eds.), Digital Imaging in Media and Education, Proceedings of the 28th Workshop of the Austrian Association for Pattern Recognition (OAGM), Hagenberg, Austria, 2004, pp. 197–204.
[26] N. Mercier, H. Valladas, G. Valladas, J.-L. Reyss, A. Jelinek, L. Meignen, J.-L. Joron, TL dates for burnt flints from Jelinek's excavations at Tabun and their implications, Journal of Archaeological Science 22 (1995) 495–509.
[27] F. Mokhtarian, M. Boberin: Curvature scale space representation, and MPEG-7 standardization, vol. 25, Kluwer academic Publishers, Dordrecht, The Netherlands, 2003.
[28] A. Razdan, D. Liu, M. Bae, M. Zhu, G. Farin, Using geometric modeling for archiving and searching 3D archaeological vessels, in: International Conference on Imaging Science, Systems, and Technology CISST 2001, Las-Vegas, 2001.
[29] D.A. Roe, British Lower and Middle Palaeolithic handaxe groups, Proceedings of the Prehistoric Society 34 (1968) 1–82.
[30] D.A. Roe, The British Lower and Middle Palaeolithic: some problems, methods of study and preliminary results, Proceedings of the Prehistoric Society 30 (1964) 245–267.
[31] R. Sablatnig, C. Menard, Computer based acquisition of archaeological finds: the first step towards automatic classification, in: P. Moscati, S. Mariotti (Eds.), the Third International Symposium on Computing and Archaeology, vol. 1, Rome, 1996, pp. 429–446.
[32] I. Saragusti, Changes in the morphology of handaxes from Lower Paleolithic assemblages in Israel, Institute of Archaeology, The Hebrew University, Jerusalem, 2002.
[33] I. Saragusti, I. Sharon, O. Katzenelson, D. Avnir, Quantitative analysis of the symmetry of artefacts: Lower Paleolithic handaxes, Journal of Archaeological Science 25 (1998) 817–825.
[34] K.L. Verosub, N. Goren-Inbar, C. Feibel, I. Saragusti, Location of the Matuyama/Brunhes boundary in the Gesher Benot Ya'aqov archaeological site, Israel, Journal of Human Evolution 34 (1998) A22.
[35] T. Wynn, Piaget, stone tools and the evolution of human intelligence, World Archaeology 17 (1985) 32–43.
[36] H. Zabrodsky, D. Avnir, Continuous symmetry measures, Journal of American Chemical Society 117 (1995) 462–473.